Verification & validation of CFD and fluid-structure-interaction simulation for digital certification of an aircraft wing

Christian Heinrich, PhD
(Boeing Deutschland GmbH, Germany);

Abstract

The aim of the presented work is to extend the building block approach as currently used in certification of aircraft structures and combine it with aerodynamic aspects. The goal of is to reduce physical test effort and shorten development time while increasing the required degree of confidence into the performance of the aircraft. Aeroelastic effects are considered to enhance the predictive level of loads by using coupled fluid-structure-interaction (FSI). FSI is considered on certification grade structural finite element models to include the changes of loads predicted by CFD with the changes in displacement.

In the development of new aircrafts, the structural building block approach and structural test pyramid is commonly employed and part of the acceptable means of compliance with the regulators on the structural side. The same approach is used here to derive more accurate values for the aerodynamic loads applied to the aircraft. To that extend the verification and validation procedures are executed on the applied CFD code along the levels of the aerodynamic test pyramid. At the bottom, coupon level simulations on 2D profiles are done that serve as verification cases. Simple closed form solutions are compared with numerical results to establish correct implementation of the mathematical equations into the computer code. These are flat plates and simple profiles solutions for laminar and turbulent flow. Also, aerodynamic closed form solutions are used. Stretching the profile in spanwise direction will be used for the validation in the element level. This closes the non-specific simulation on the aerodynamic side.

The next levels serve for validation with increasing complexity based on real geometries for later application. Here the simulation results are compared to the experimental results of a 3D wing geometry under turbulent flow as well as fluid flow around high lift devices (detail level). Also, fluid-structure-interaction of vortex shedding around a cylinder and elastic member is considered.

Finally, the aeroelastic deformations are presented at the component level of the test pyramid. Here a composite wing structure is deforming under aerodynamic loads and thus altering the flow characteristics. Considering the

interaction between fluid and structure and evaluating loads based on the deformed structure is expected to improve the accuracy of the numerical predictions. Numerical and experimental results are compared with each other to complete the validation process. By consistently applying verification and validation from the bottom to the top of the structure and aerodynamic test pyramid, confidence can be placed in the predictive capability of the models and ultimately a reduction in test efforts can be attempted.

In comparison to other fluid-structure-interaction investigations, the present analysis is focused on large deformation and deflection on a complex structural model. The methodology is presented at the example of the outer wing of a glider aircraft which shows a tip deflection of 0.9 meters over a 5 m wing span. Secondly, no simplification of the structural model is performed and hence the structural model with the resulting load can be used as is for structural certification.

1. Background

Certifying aircraft structures is expensive and time consuming. It is in principle possible to certify in aircraft structure purely by test as stated for example in the AC 25.307-1 [1]. However, that would increase cost and time even further. Nowadays a combination of test and analysis is used, depending on the level of knowledge and past experience. In order reduce the effort in time, money and other resources a certification supported by Modelling and Simulation (M&S) is desired. This is in principle not different compared to current approaches except for extend that analysis replaces physical tests. Other names for similar approaches are “Certification by Analysis” [2] and “Smarter Testing” [3]. In the context of regulations, there is currently the draft available of the EASA Certification Memorandum 014 - Modelling & Simulation – CS-25 Structural Certification Specifications [4]. The ideas of the CM are also expected to be contained in the upcoming work of the ASME VVUQ 90 Committee “Verification, Validation, and Uncertainty Quantification in Computational Modelling of Airframe Structures”.

The CM-S 014 divides the tasks for certification by aid of M&S roughly into verification, validation and uncertainty quantification:

- Verification is concerned with the correct implementation of the math and theory implemented into a computer program. Verification is typically checked with the aid of closed form solutions and small or unit cell sized models. It is conceptually also possible to perform verification against other, already verified computer codes. The question that is asked when performing verification is “Am I solving the equations correctly”. At first glance verification appears to be a straight forward task as it focuses more on correct execution and implementation of a theory, which would be considered a more straight-forward activity compared to conceiving a new theory. However, the vast amount of possible verification cases possible and the level of care required for certification applicable verification should not be underestimated.

- Validation is concerned with the connection between the analysis models and theory to the real physical world. Here more complex models (compared to the verification cases) are compared to physical tests. The question to be asked when performing validation is “Am I solving the correct equations?”
- The final part of M&S is uncertainties and errors which is related to uncertainty quantification (UQ). This part will not be addressed in this contribution but would be required for a complete M&S based certification approach. The topic of uncertainties and errors includes how to treat uncertainties in the experimental results, uncertainties in the inputs of the analysis and sensitivity analysis.

In the certification of aircraft structures a building block approach is commonly used. The building block approach for aircraft structures is given in Figure 1 [5], [6]. The certification builds up though several levels with increasing complexity: coupons, elements, details, subcomponents and components:

(1) Coupons represent the simplest entities and they are used for the determination of material values and allowable.
(2) Elements are more complex and do not represent isolated behaviour that can be attributed to a single effect. For a composite structure, a single or multiple layer of material oriented in the same direction represent a coupon, while several layers with different orientations represent an element. Elements and coupons are generic and not specific to a certain structure.
(3) Details are a collection of elements that represent an isolated, yet specific structural feature.
(4) Subcomponent are a collection of details, that don’t represent a full component yet.
(5) Components represent major parts of the aircraft.

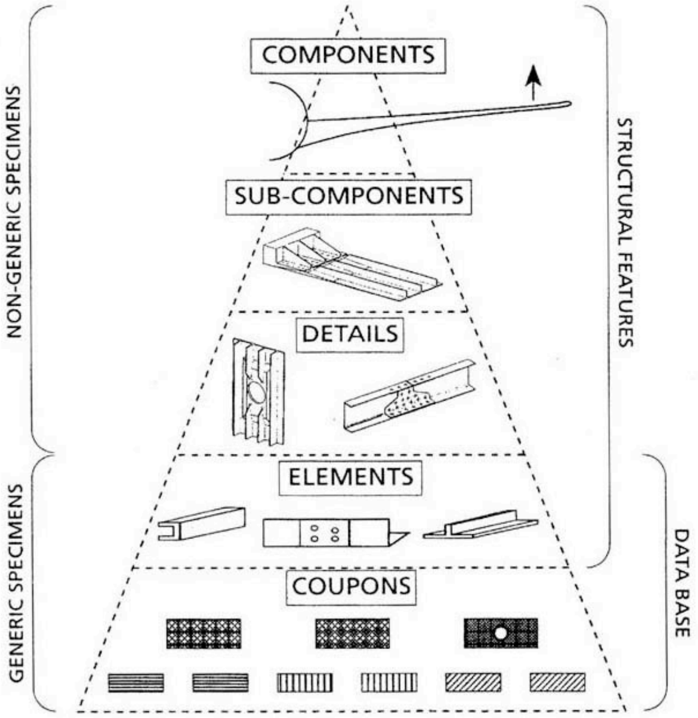

Figure 1: Building block approach for certification of aircraft structures as given by AMC 20-29/ AC 20-107B

While the use of analyses is already described in the applicable guidance material, such as the AC 25.307-1, the CM-S 014 [4] explicitly builds up the test pyramid in the context of test and analysis separately and shows how they interact at the different levels. The test pyramid including test and analysis is given in Figure 2. The lower levels of the pyramid represent the verification activities. Here simulation results are compared to known closed form solutions. The intermediate and upper levels of the pyramid represent the validation activities, where the simulation results are compared with experimental results. Finally, the upper and top level of the pyramid represent the certification activities.

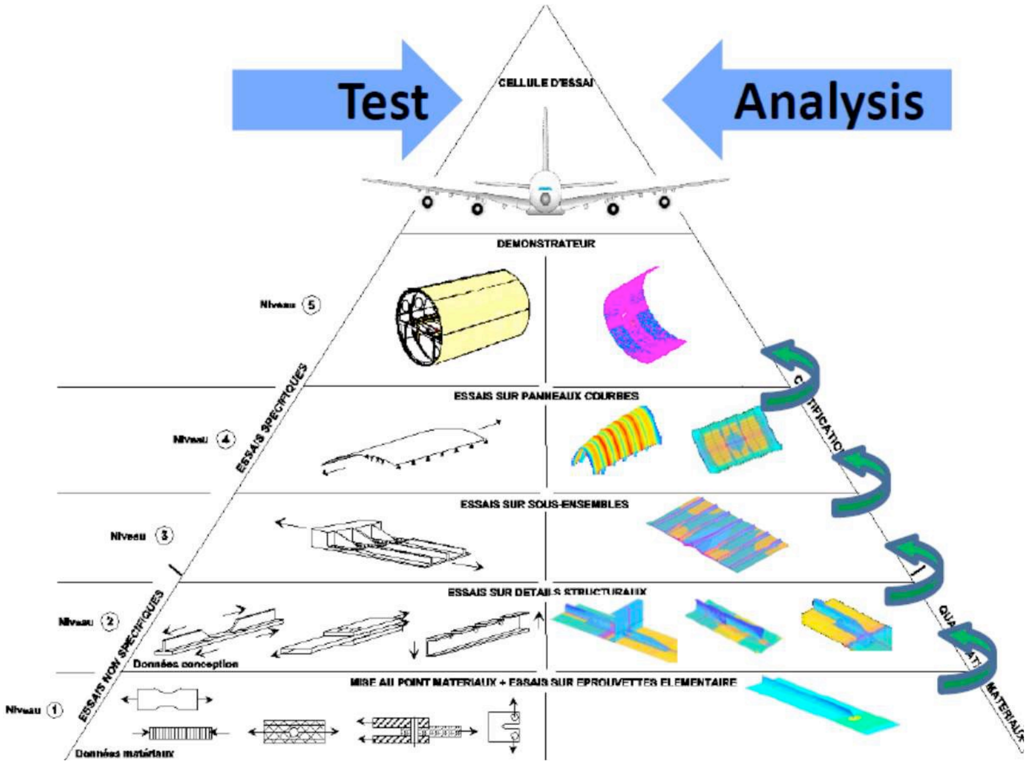

Figure 2: Test and analysis pyramid as per CM-S 014

All information presented so far related to aircraft structures and the beforementioned documents apply to structural certification. Next, the ideas are extended to the fluid-mechanics domain in Figure 3. The CM-S 014 and cited guidance material applies to structural application and the presented test pyramid is therefore considered a new suggestion at this point.

Similar to the already presented certification pyramid, there are five levels from coupon to component. Different tests and analyses are performed from bottom to top to cover the cycle from verification, to validation and to certification.

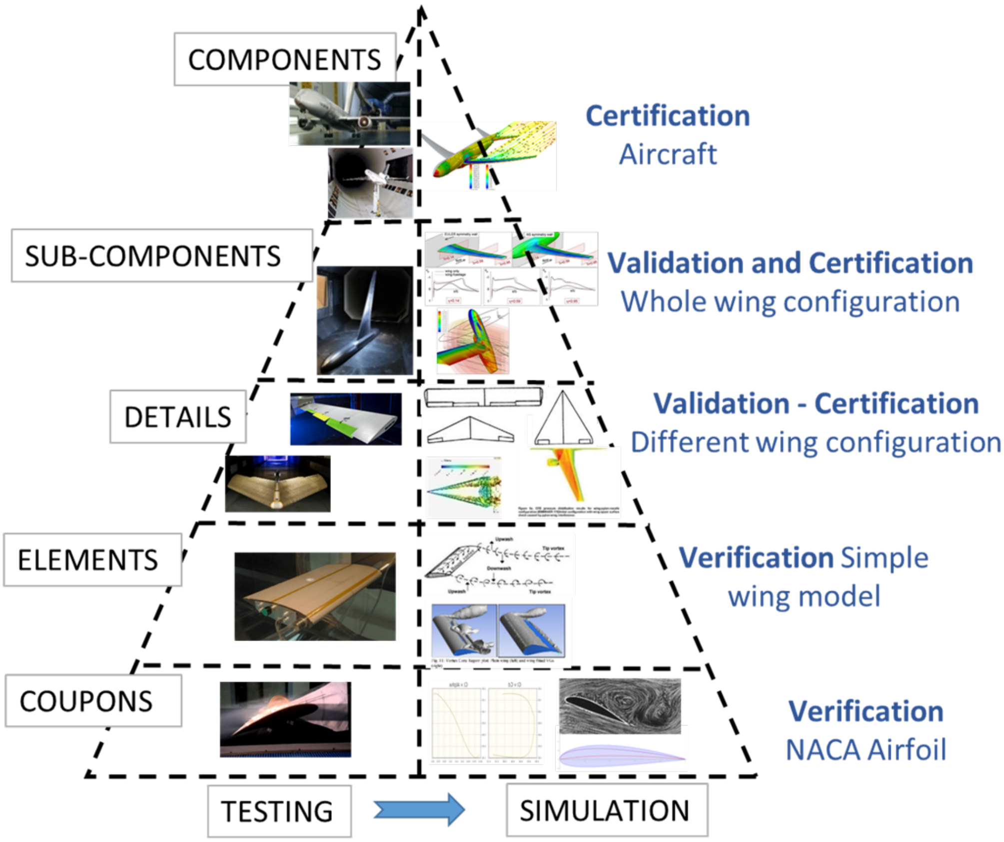

Figure 3: Test and simulation pyramid for fluid-dynamics

The different analyses along the certification pyramid are in detail described in Section 2 and summarized in Table 1.

While almost all of the presented cases have been investigated many times in the literature, they still need to be repeated with the applied software, workflow and settings among all levels of the test pyramid. This is necessary in order to establish credibility in the results obtained at the very top of the pyramid and make the process suitable for a Modelling and Simulation supported certification.

The software used in this study is Hexagon Cradle CFD ScFLOW [7] for the CFD solver, and MSC CoSim [8] for FSI analysis.

This paper focuses on the fluid-dynamics test pyramid as no guidance material exist that explicitly presents the fluid-dynamics test pyramid in the way that it is done for the structural aspects in [4], [5] and [6]. When using the full FSI at the top of the test pyramid it is implicitly assumed, that the verification and validation process has also been completed on the structural side.

2. Cases comprising the different level of the test pyramid

Next, the different cases that were investigated are described in more detail. The cases are summarized in the following table 1.

Table 1: Verification, validation and certification cases along test pyramid

Level	Name	CFD only/ FSI	Purpose	Ref.	Result
Coupon	Flat Plate Blasius Solution	CFD only	Verification	[9] [10]	Passed
Coupon	Flat plate turbulent transition	CFD only	Verification	[11] [10]	Passed
Coupon	2D wing section Lift vs. Drag	CFD only	Validation	[12]	Passed
Coupon	2D wing section pressure distribution and wake	CFD only	Validation	[13]	Passed
Coupon	2D wing section with structural coupling	FSI	Verification	[14]	Passed
Element	Moving membrane	FSI	Verification	[15]	Passed
Element/ Detail	Finite wing	CFD only	Validation	[16]	Passed
Subcomponent	High lift device	CFD only	Validation + Certification	[17]	Work ongoing
Component	Finite wing with structural coupling	FSI	Certification	-	Work ongoing

a. Flat Plate Blasius Solution

In the first verification case the Blasius solution is investigated [9]. In this analysis case, a constant laminar fluid flow impacts a flat plate. At the interface between the flow and the plate is a no-slip / zero-velocity boundary condition. As a result, a boundary layer is building up. This is schematically shown in Figure 4. Viscous flow is assumed.

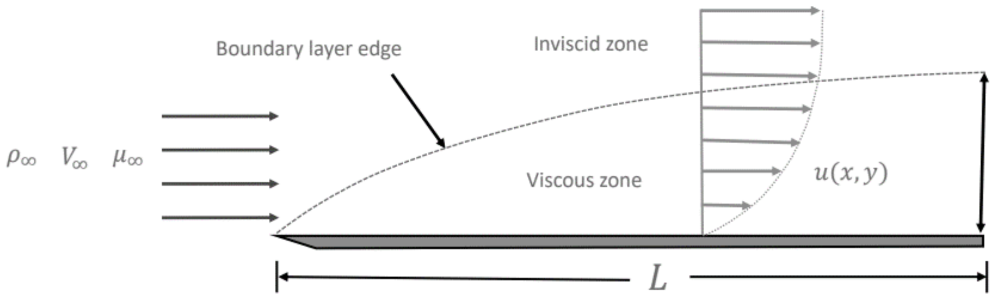

Figure 4: Blasius flat plate solution schematically

The results of the analysis are shown in Figure 5**Error! Reference source not found.** in the form of velocity profiles at different stations along the x-direction. In order to achieve a self-similar solution a non-dimensionalized format is used, with the non-dimensionalized coordinate η along the y-axis and the non-dimensionalized velocity u/U along the x-axis.

Numerical results compare very well with theoretically predicted values.

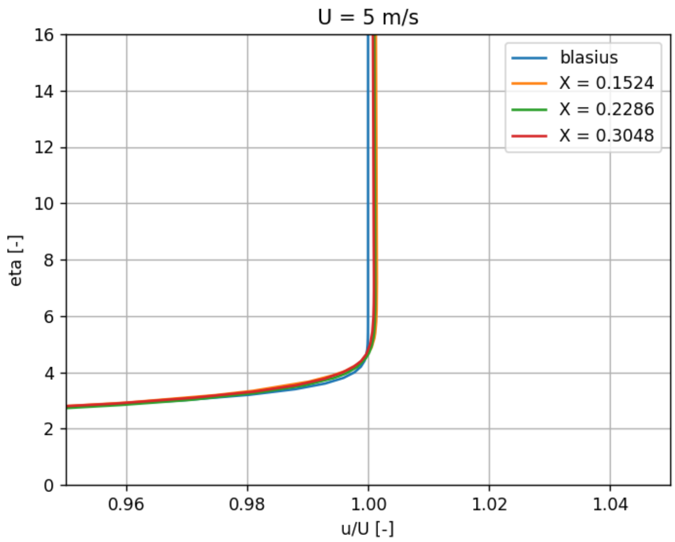

Figure 5: Flat plate viscous flow - Blasius solution and numerical results along different stations

b. Flat plate – Turbulent transition

Next the same problem of a flat plat is considered with turbulent flow. Therefore, the SST-k-ω turbulence model is used [18]. The same turbulence model will be used for all further cases in this paper.

The general physical behaviour of the problem is shown in Figure 6 [19]. Initially a laminar boundary layer forms in the same manner as in the Blasius-solution as given above. What follows is a transition to turbulent boundary that will be eventually fully established.

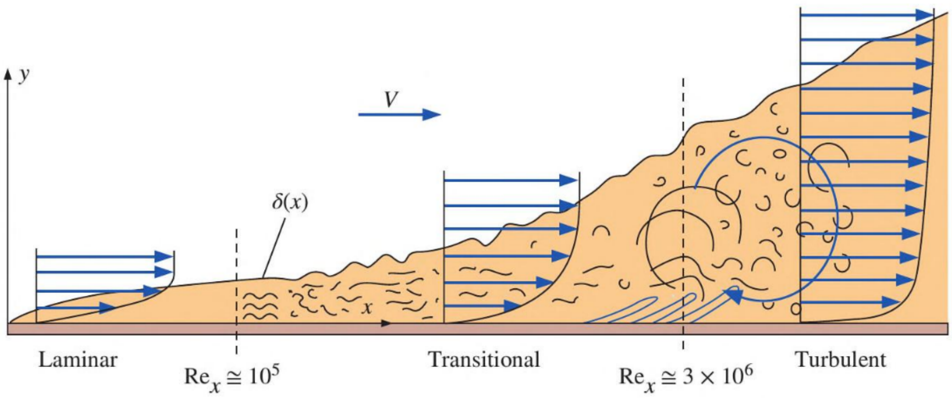

Figure 6: Laminar to turbulent boundary layer transition [19]

A comparison between the simulation result and analytical solution are presented in Fig7. Again, a non-dimenzionalized form is chose for the velocity profile. This time the non-dimenzionalized velocity u+ over the non-dimenzionalized wall distance y+ in log form.

The results show a very good agreement in the laminar sublayer (1) y+ < 5 as well as in the logarithmic region (3) at y+ > 30. In the transition region in-between (2) a blending function between both profiles is used.

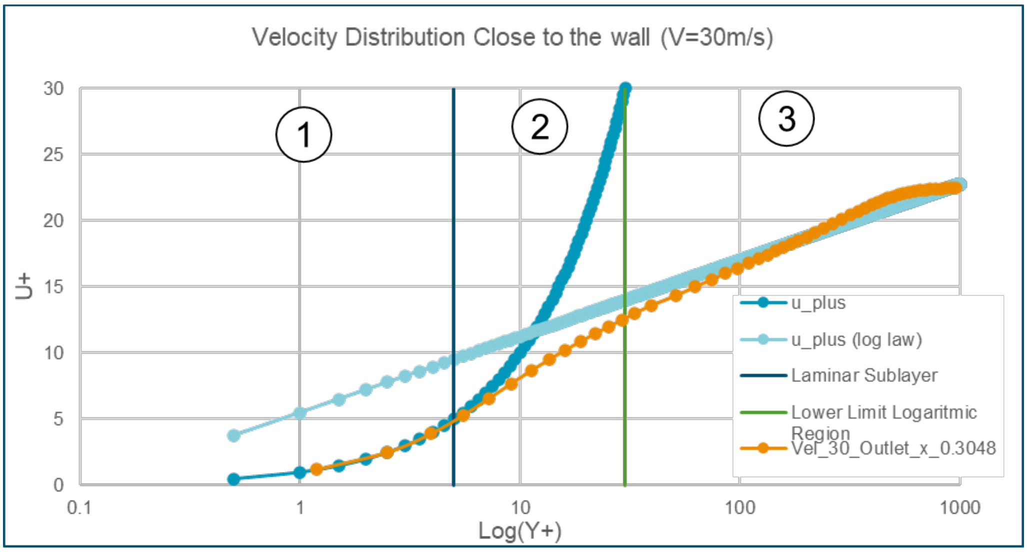

Figure 7: Results laminar to turbulent transition of boundary layer

c. 2D Airfoil – Lift vs. Drag

Next, the flow around a 2-dimensional airfoil as shown in Figure 8 is investigated. The airfoil is of type NACA 4412. The experimental results are taken from [12].

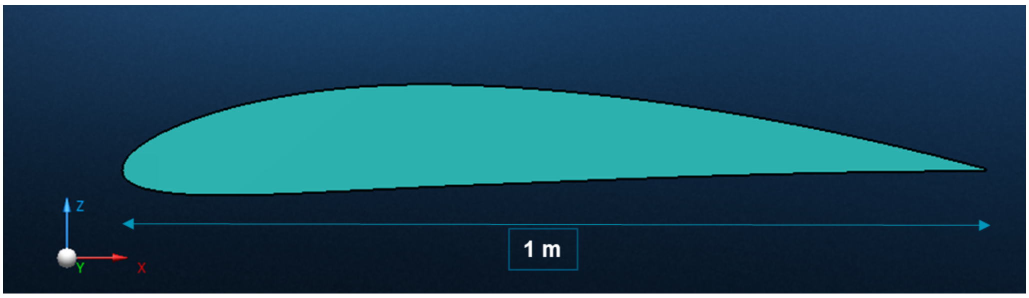

Figure 8: NACA 4412 airfoil

The comparison between experimental and analytical results for lift coefficient vs. angle of attack are given Figure 9. In the linear regime, experimental and numerical results agree very well. However, the stall angle is too optimistic and overpredicted. This is most likely caused by inaccuracy in the inflow turbulence level (which was assumed too high with 5% instead of 0.1%)

combined with a non-sufficient mesh refinement, that would be required to resolve back-circulation and similar effects that occur at stall. For the currently intended application (FSI of elastically deforming wing), this shortcoming in predictive capability is acceptable as the FSI case are not operated near the stall point but at moderate angles of attack.

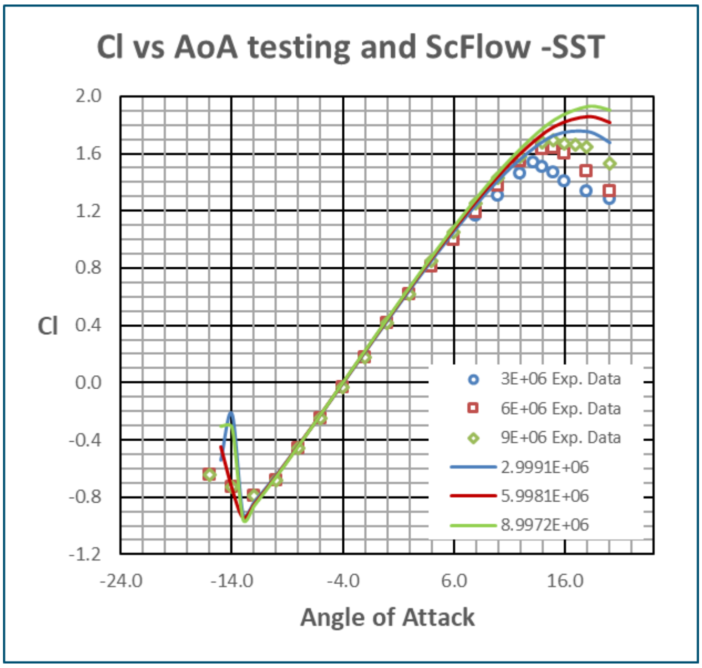

Figure 9: Lift coefficient vs. angle of Attack

The comparison between experimental and numerical results for drag coefficient vs. lift coefficient is given in Figure 10. As can be seen, the drag coefficient is significantly overpredicted. This is most likely due to the assumption of fully turbulent flow in the simulation. While the flow around the air foil contains significant laminar portions. It should be noted that the drag coefficient is an order of magnitude smaller, compared to the lift and or structural applications of less interest. The use of an additional transition model is possible, but the increase computation effort is outweighing the increase in predictive accuracy.

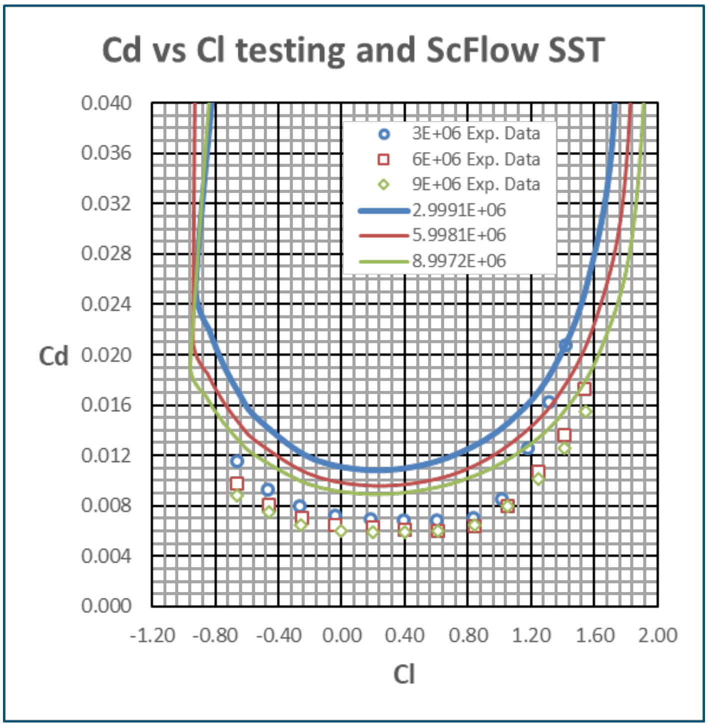

Figure 10: Drag vs lift coefficient

d. 2D Airfoil – Pressure distribution and wake

A similar investigation as presented before is repeated for a different airfoil. Here the flow around and behind a NACA 0012 airfoil is investigated. The pressure distributions are compared against measurements on the suction side of the profile. The results are presented in Figure 11, Figure 12 and Figure 13 for 0°, 10° and 15° angle of attack, respectively. It can be seen, that the pressure distribution matches very well.

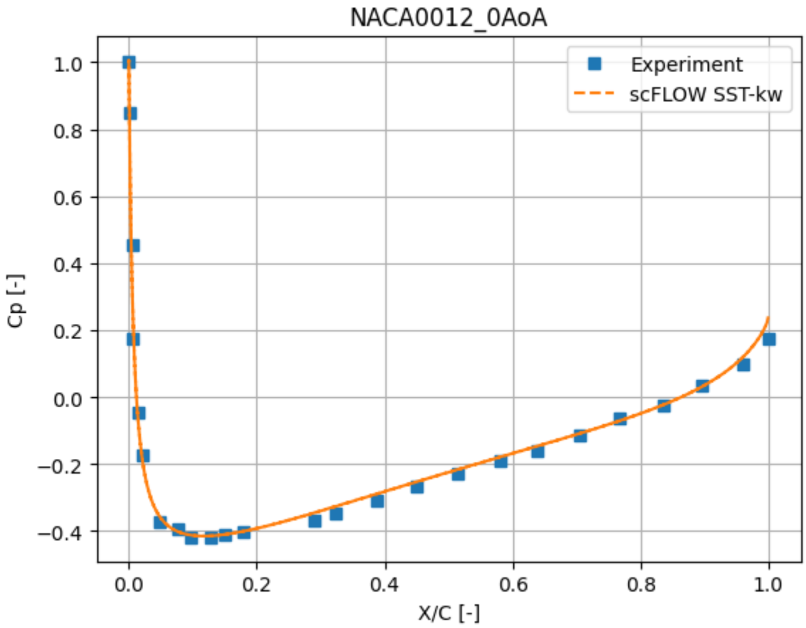

Figure 11: NACA 0012 - pressure distribution along the chord for 0° angle of attack

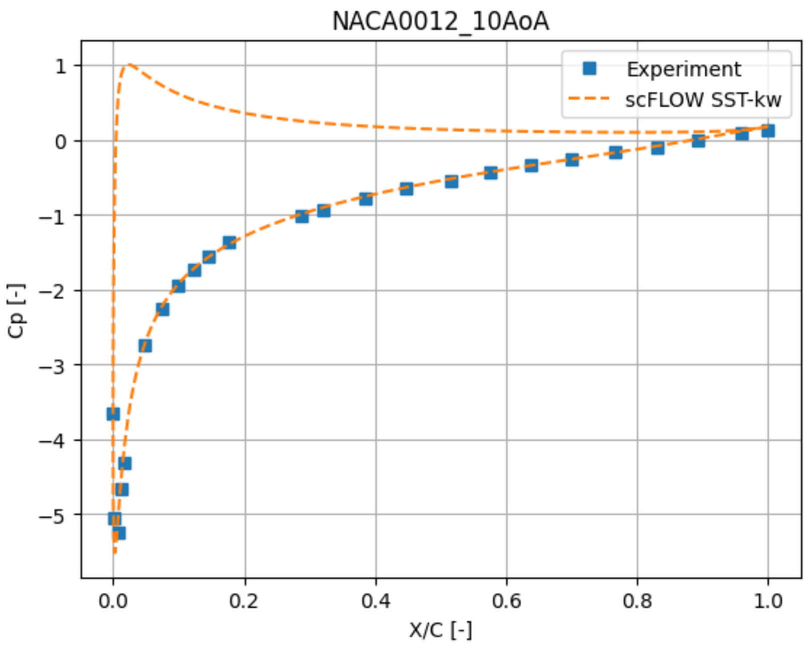

Figure 12: NACA 0012 - pressure distribution along the chord for 10° angle of attack

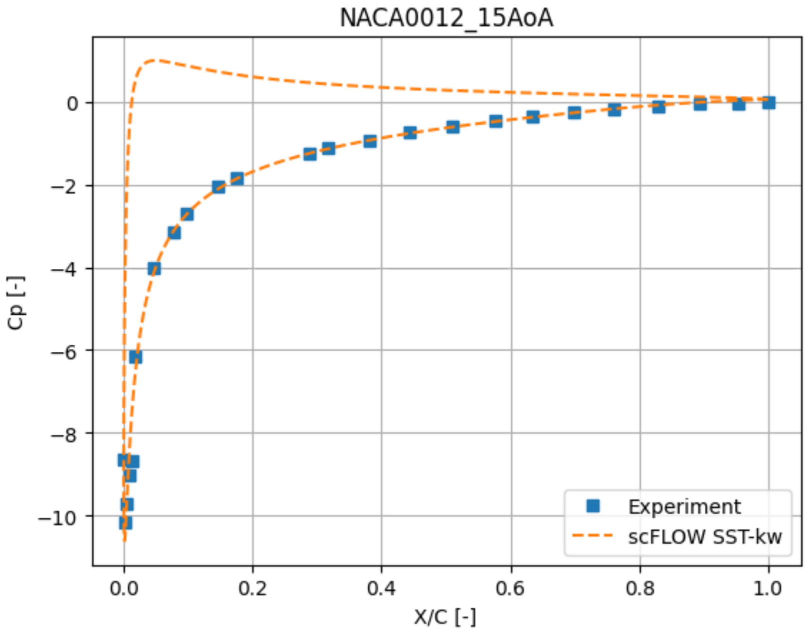

Figure 13: NACA 0012 - pressure distribution along the chord for 15° angle of attack

For the same airfoil the flow in the wake was investigated. The mesh and velocity in x-direction are shown in Figure 14 together with the different measurement stations.

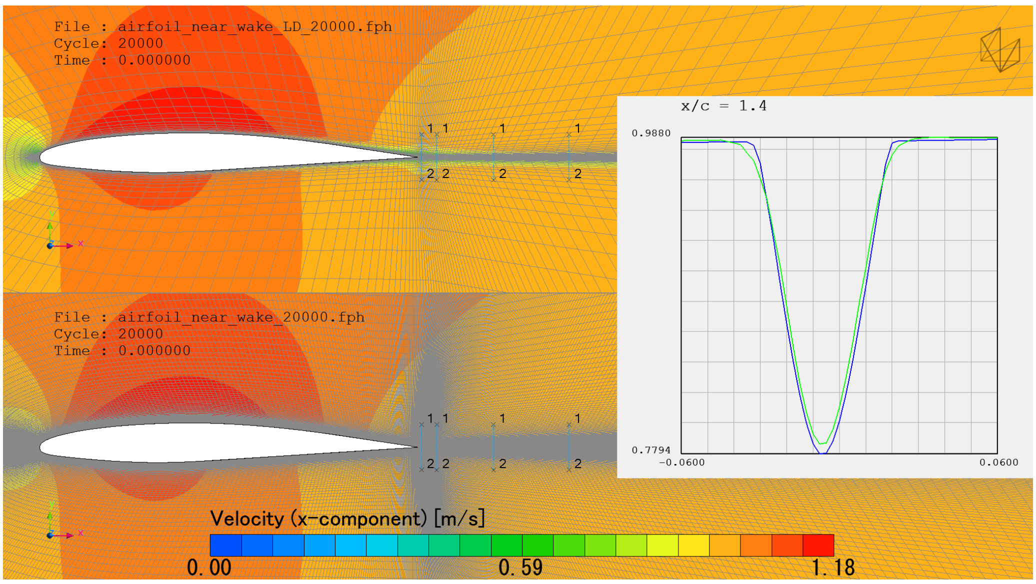

Figure 14: Velocity distribution in wake of NACA 0012 airfoil

In Figure 15 the evolution of the velocity profile in the wake of the NACA 0012 profile is compared between experimental and numerical results. The x-axis shows the velocity in x-direction, normalized by the free stream velocity in x -direction. The y-axis shows the y-coordinate normalized by the airfoil chord. Dots mark experimental results and solid lines indicate numerical results. Velocity profiles are investigated at different axial positions downstream of the airfoil. Here x/c=1.01 is right behind the airfoil and x/c=3 is three chord lengths away. With increasing distance from the airfoil, the gradients in the velocity profile reduce and a free stream velocity distribution is achieved.

Overall the experimental and numerical results agree well. For structural evaluations, the values between x/c=0 and x/c=1.0 are correct.

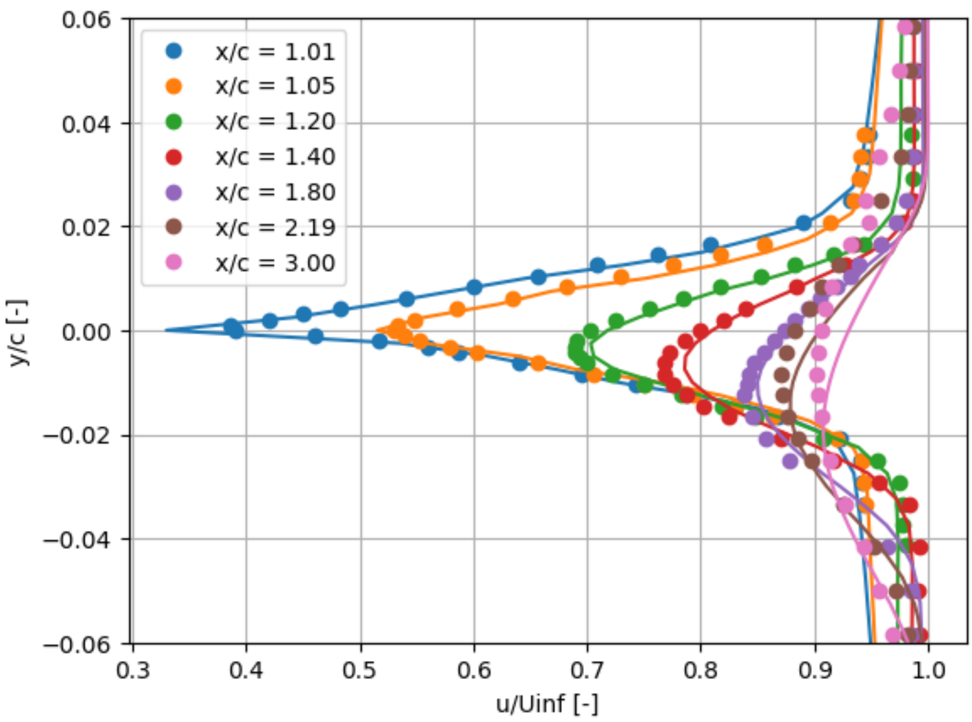

Figure 15: NACA 0012 velocity profile in wake

e. Static aeroelasticity - 2D airfoil on spring

The final case to be investigated on the coupon level is a verification case for the aeroelastic capabilities. Here a 2D airfoil on a spring is considered. The example is a standard one in many text books on aeroelasticity (see for example [14]). The principle setup is presented in Figure 16. For the airfoil the aforementioned NACA 4412 is employed. A 2D airfoil with a given center of gravity is hinged to a rotational spring. The airfoil and spring will attain a static equilibrium.

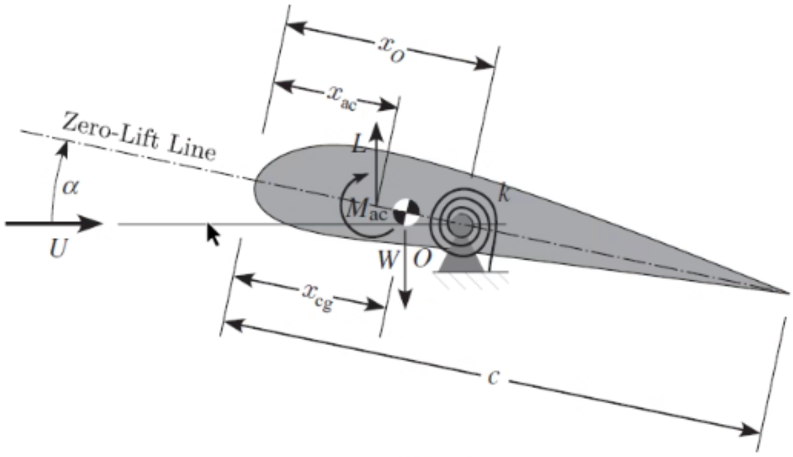

Figure 16: 2D airfoil with torsional spring [14]

A numerical solution was obtained using two different methods:

(1) Adding a spring directly in Hexagon Cradle CFD scFLOW and using the rigid body movement feature [7]
(2) Adding a spring to a Nastran and performing a co-simulation using MSC CoSim [8]. For this case the resulting CFD and FE domain are shown in Figure 17.

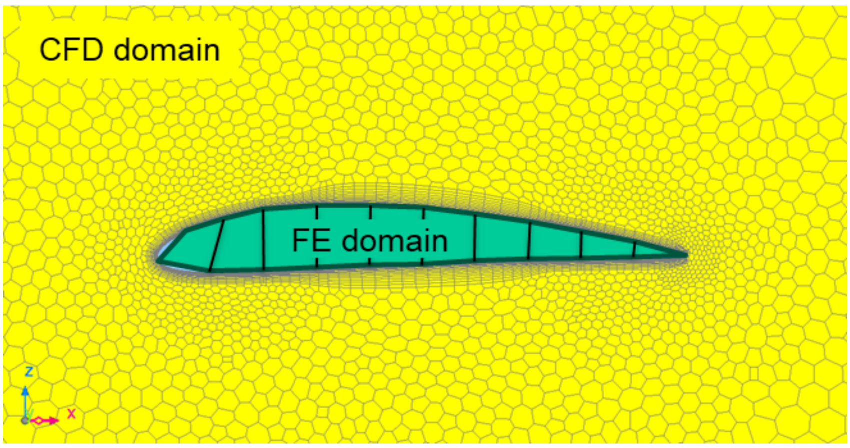

Figure 17: CoSim simulation of 2D wing on torsional spring

The results of the analysis are given in Figure 18. Both, the pure Cradle CFD / scFLOW approach and the CoSim approach converge to the same value. CoSim represents here a "pseudo-transient" simulation and accordingly the transient response between CoSim and pure CFD is different. The numerical and analytical results are deviate by about 2.5 %. This is due to the linearization of airfoil characteristics (Cl and Cm vs. alpha) on which the analytical solution is based.

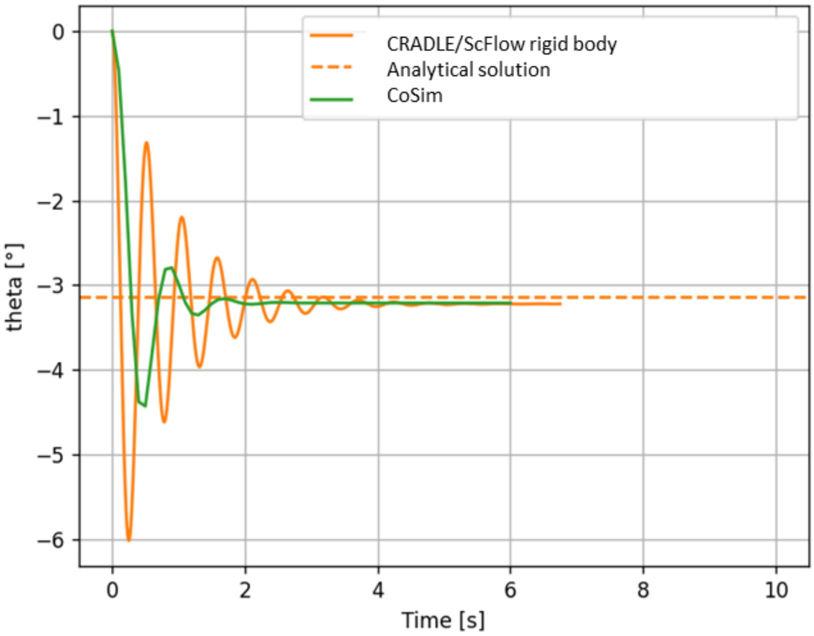

Figure 18: Results aeroelasticity single degree of freedom airfoil

f. Flapping membrane

Turek and Hron [15] proposed a benchmark to assess the performance of fluid-structure-interaction solvers. Here a membrane is placed behind a cylinder in a tunnel filled with a viscous fluid in laminar flow conditions (Re_D = 100 – 200). At these velocities, the cylinder induces a Kármán vortex street and the highly flexible membrane deforms according to the shedding of the vortices. The cylinder is located slightly off the middle line of the test tunnel. As a result, minor lift is induced on the cylinder.

The general setup and parameters are given in Figure 19, including the investigated cases FSI2 and FSI3.

Figure 20 shows the velocity profile in the symmetry plane around the cylinder and membrane. Time t = 0 seconds (top), shows the initial flow field coming from a rigid membrane, with which he FSI starts. At time t = 9.5 seconds (bottom) the vortex street is fully developed and the membrane is deforming accordingly.

Figure 21 and Figure 22 show the tip displacement (in X and Y) (point A in Figure 19) as well as the aerodynamic forces over several cycles. For FSI 2 (Re = 100, Figure 21) the displacements and forces are well calculated. However, the frequency is under predicted. At higher inflow velocity in FSI 3 (Re = 200, Figure 22) the frequencies match well. Magnitudes in displacement are underpredicted. Overall correlation is good. It should also be noted, that the reference solution itself is only derived numerically and that 19 years ago.

Therefore, no clear answer can be given to which solution, the one from Turek and Hron or the one in the current paper, is actually more correct.

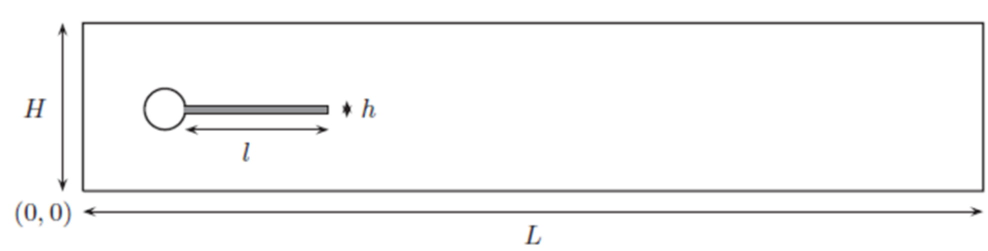

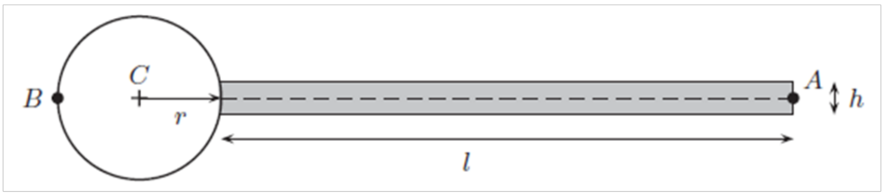

parameter	FSI1	FSI2	FSI3
ϱ^s $[10^3 \frac{\mathrm{kg}}{\mathrm{m}^3}]$	1	10	1
ν^s	0.4	0.4	0.4
μ^s $[10^6 \frac{\mathrm{kg}}{\mathrm{ms}^2}]$	0.5	0.5	2.0
ϱ^f $[10^3 \frac{\mathrm{kg}}{\mathrm{m}^3}]$	1	1	1
ν^f $[10^{-3} \frac{\mathrm{m}^2}{\mathrm{s}}]$	1	1	1
U $[\frac{\mathrm{m}}{\mathrm{s}}]$	0.2	1	2

parameter	FSI1	FSI2	FSI3
$\beta = \frac{\varrho^s}{\varrho^f}$	1	10	1
ν^s	0.4	0.4	0.4
$\mathrm{Ae} = \frac{E^s}{\varrho^f \bar{U}^2}$	3.5×10^4	1.4×10^3	1.4×10^3
$\mathrm{Re} = \frac{\bar{U}d}{\nu^f}$	20	100	200
$\bar{U}$	0.2	1	2

geometry parameters		value [m]
channel length	L	2.5
channel width	H	0.41
cylinder center position	C	$(0.2, 0.2)$
cylinder radius	r	0.05
elastic structure length	l	0.35
elastic structure thickness	h	0.02
reference point (at $t = 0$)	A	$(0.6, 0.2)$
reference point	B	$(0.2, 0.2)$

Figure 19: Flapping membrane setup

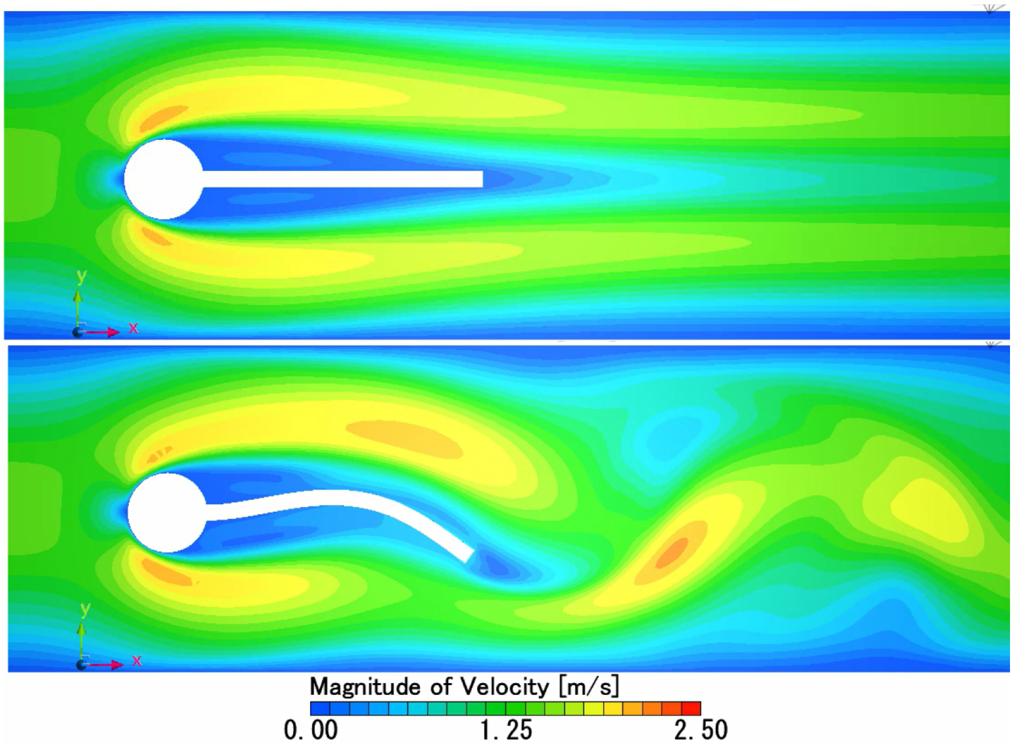

Figure 20: Flapping membrane velocity field (top t=0 s, bottom t=9.5 s)

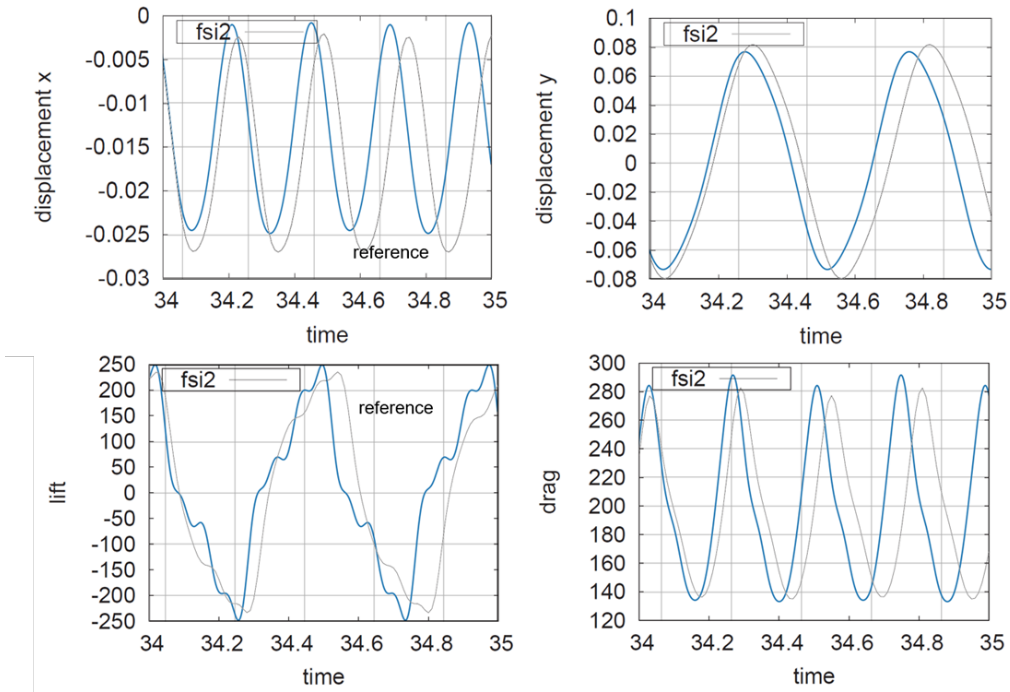

Figure 21: Flapping membrane, results FSI 2

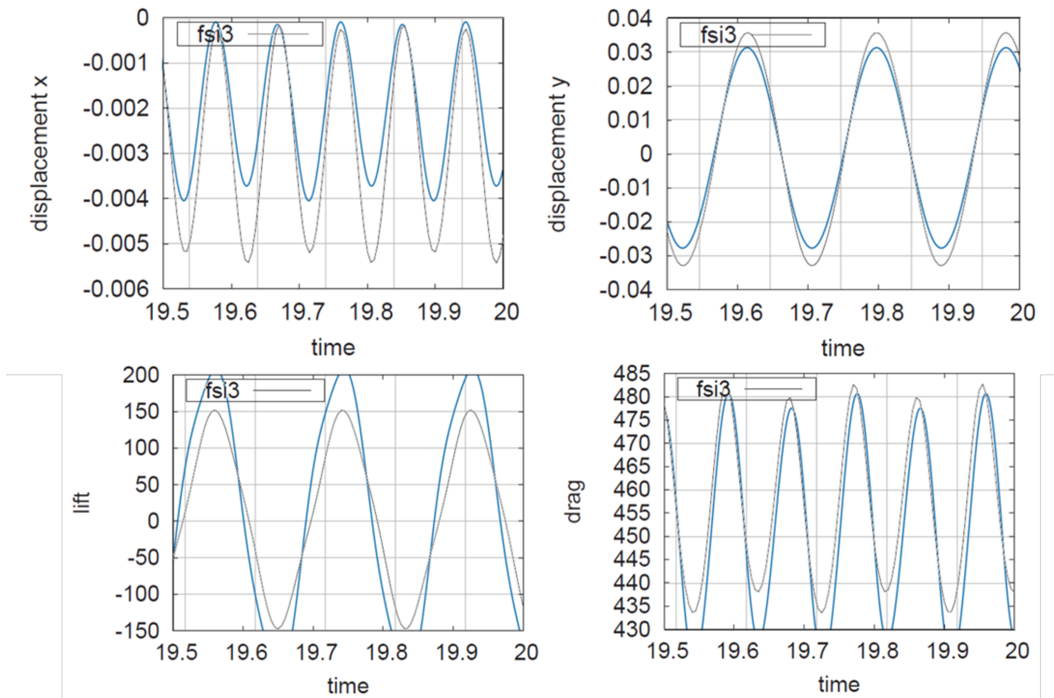

Figure 22: Flapping membrane, results FSI 3

g. Finite Wing

The next investigation fits into the element or detail level of the test pyramid. The lift of a finite wing, attached to a generic fuselage and the interaction of wing and fuselage are compared between experimental and numerical results [16].

Photographs of the general setup are shown in Figure 23 and the geometric description of tested wing is shown in Figure 24.

Two types of wings are investigated: an elliptical and a rectangular wing.

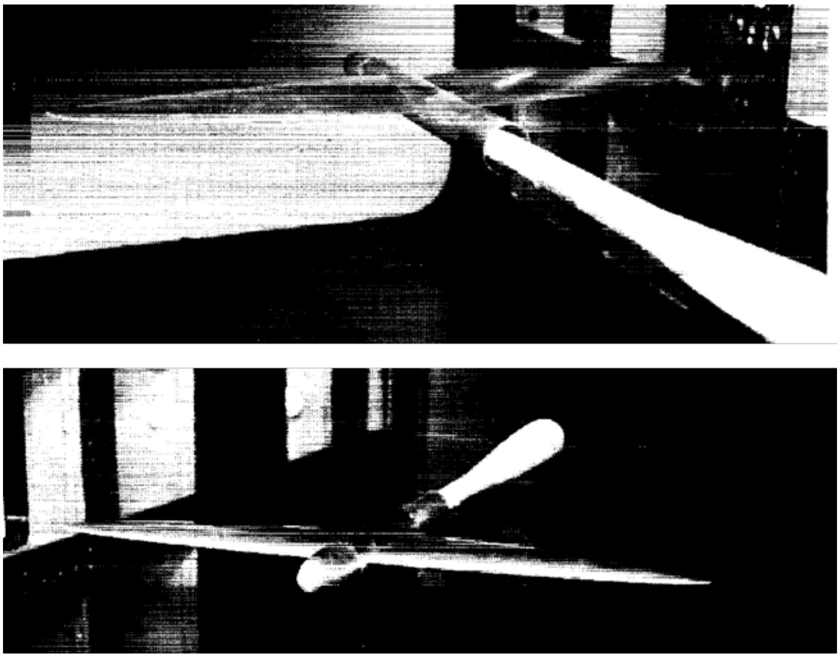

Figure 23:Test for finite wing [16]

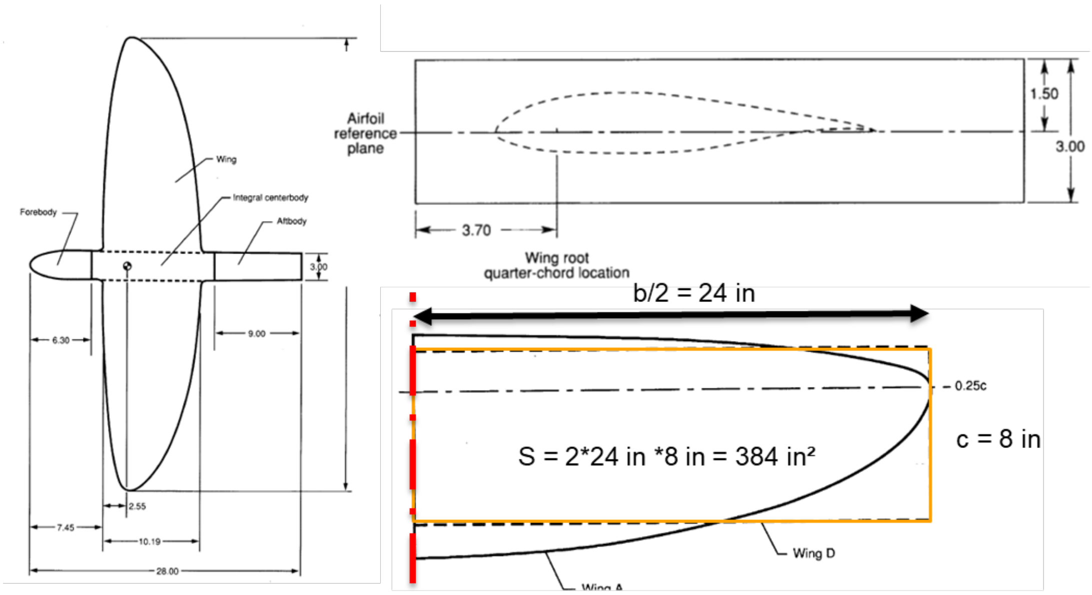

Figure 24: Geometry description of finite elliptic (wing A) and flat wing (wing D) and airfoil cross section

At the top of Figure 25 the pressure distribution as determined by simulation is shown for the elliptical and rectangular wing. It can be seen that a rectangular wing induces a significantly larger trailing edge vortex compared to an elliptical wing as expected.

In the middle of Figure 25, lift coefficient vs. angle of attack are compared between experimental and numerical results for the two wing types and at the bottom the same is given for lift coefficient vs. drag coefficient. In all cases the numerical results compare very well with the experimental ones.

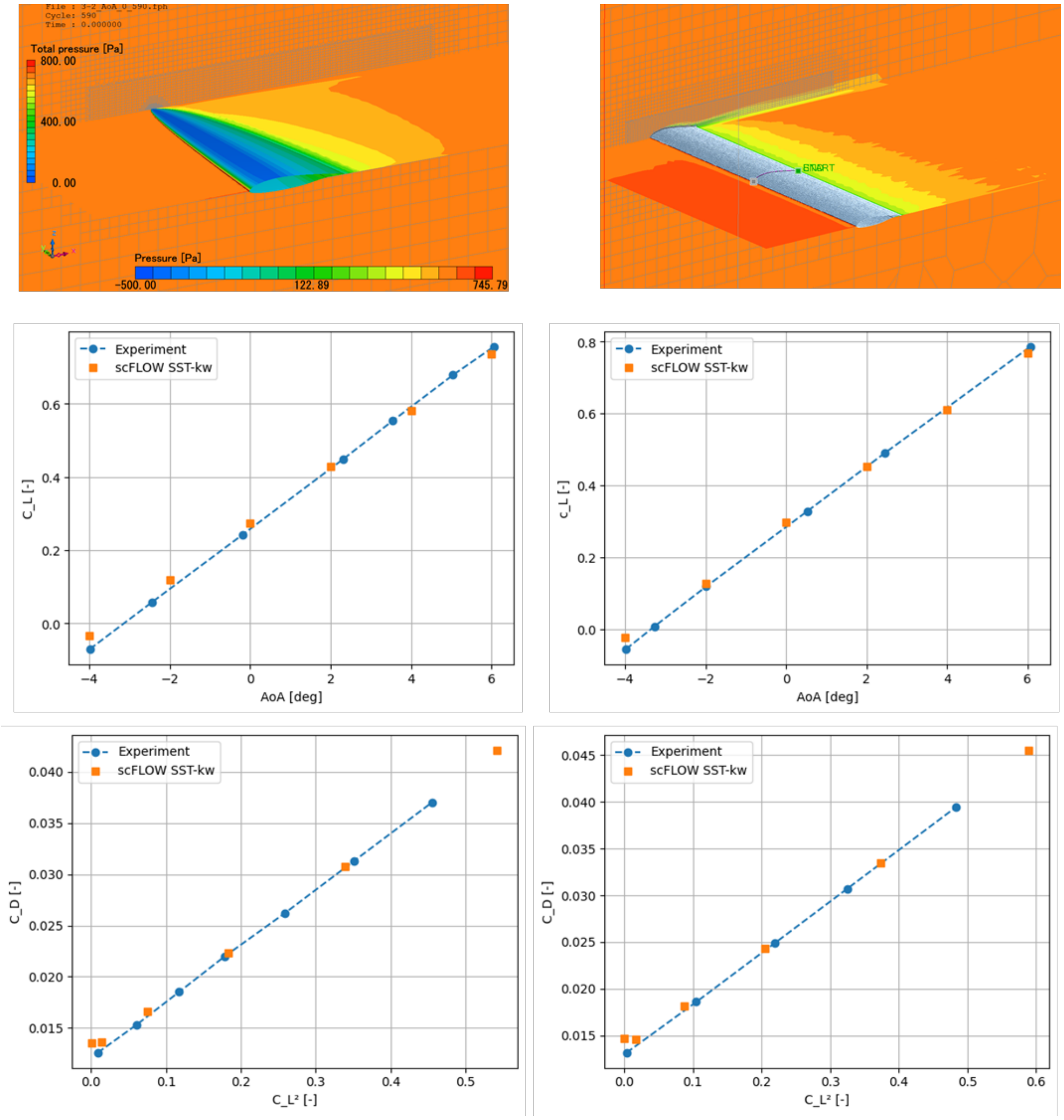

Figure 25: Finite wing - pressure distribution, lift vs. angle of attack and lit vs. drag for elliptical and rectangular cross section

h. High lift device

At the subcomponent level of the test pyramid high lift devices are investigated. The AIAA CFD High Lift Prediction Workshop is an excellent resource and in the following the results from the 3rd workshop are used [17]. The JAXA model without nacelles is considered. The test setup is shown in Figure 26.

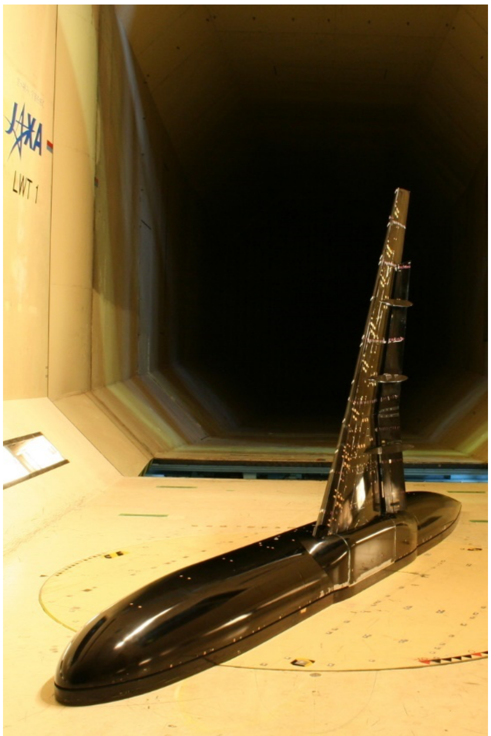

Figure 26: High lift prediction workshop, test setup

The comparison between experimental and numerical for lift coefficient and angle of attack for the workshop case 1 are given in Figure 27. “JAXA JSM Case 1” denotes the experimental results and the other data points denote numerical results with different solver settings. At low angles of attack, experimental and numerical values agree well. At higher angles of attack, numerical results are too conservative/ low. It was identified that in the provided meshes problems exist in some prism layers near the walls of the flaps producing convergence issues at high angles of attack that still require further mesh adjustment.

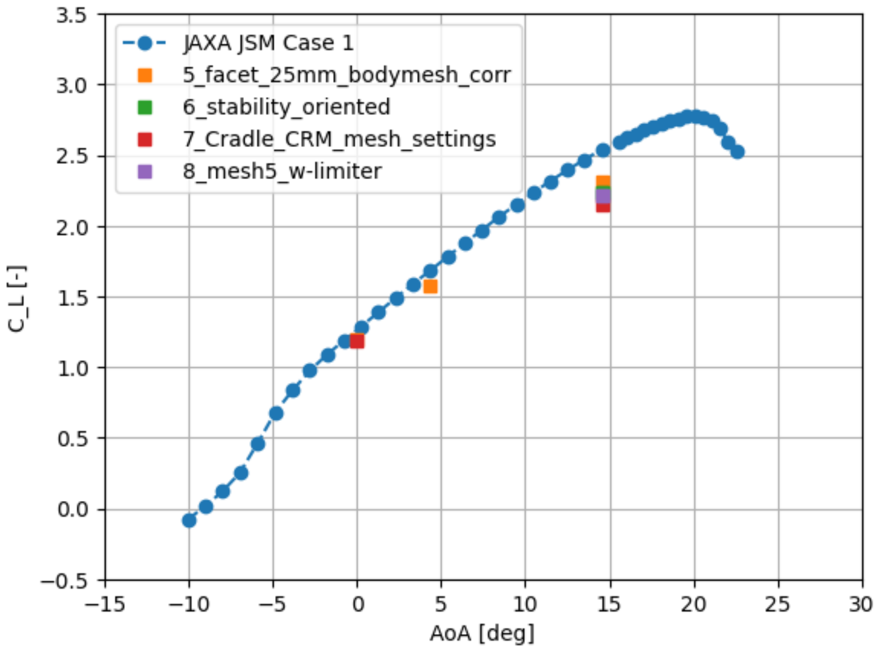

Figure 27: Experimental and numerical results for workshop case 1

The pressure distribution at different stations along the wing is give in Figure 28 and Figure 29 at 15 deg angle of attack. Generally, trends are followed well and the pressure distribution around the wing is predicted well. Predictions around the slat and top of the flap are least accurate. These are the areas with the most complex flow patterns.

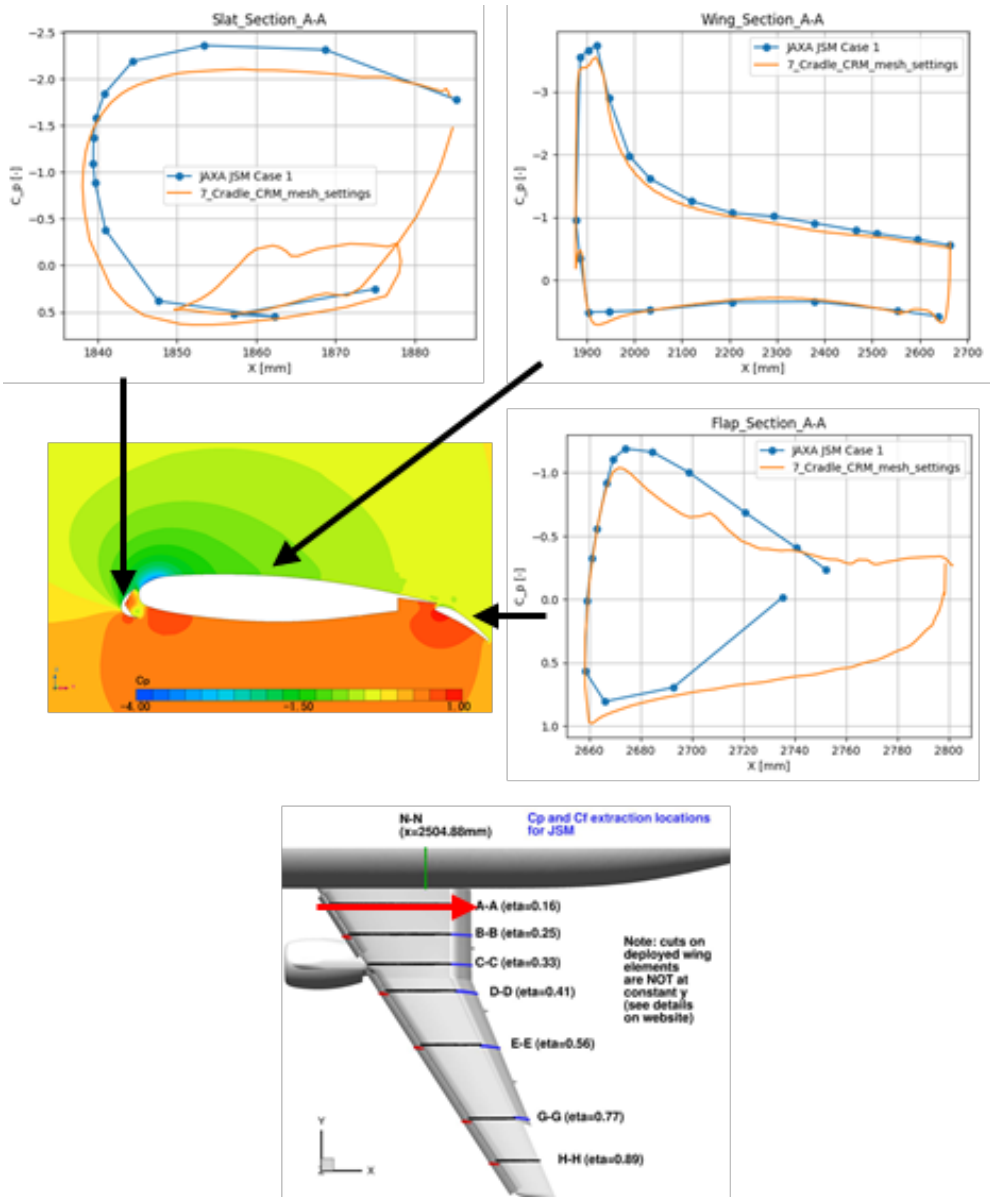

Figure 28: High lift prediction, station A-A at 15 deg AoA

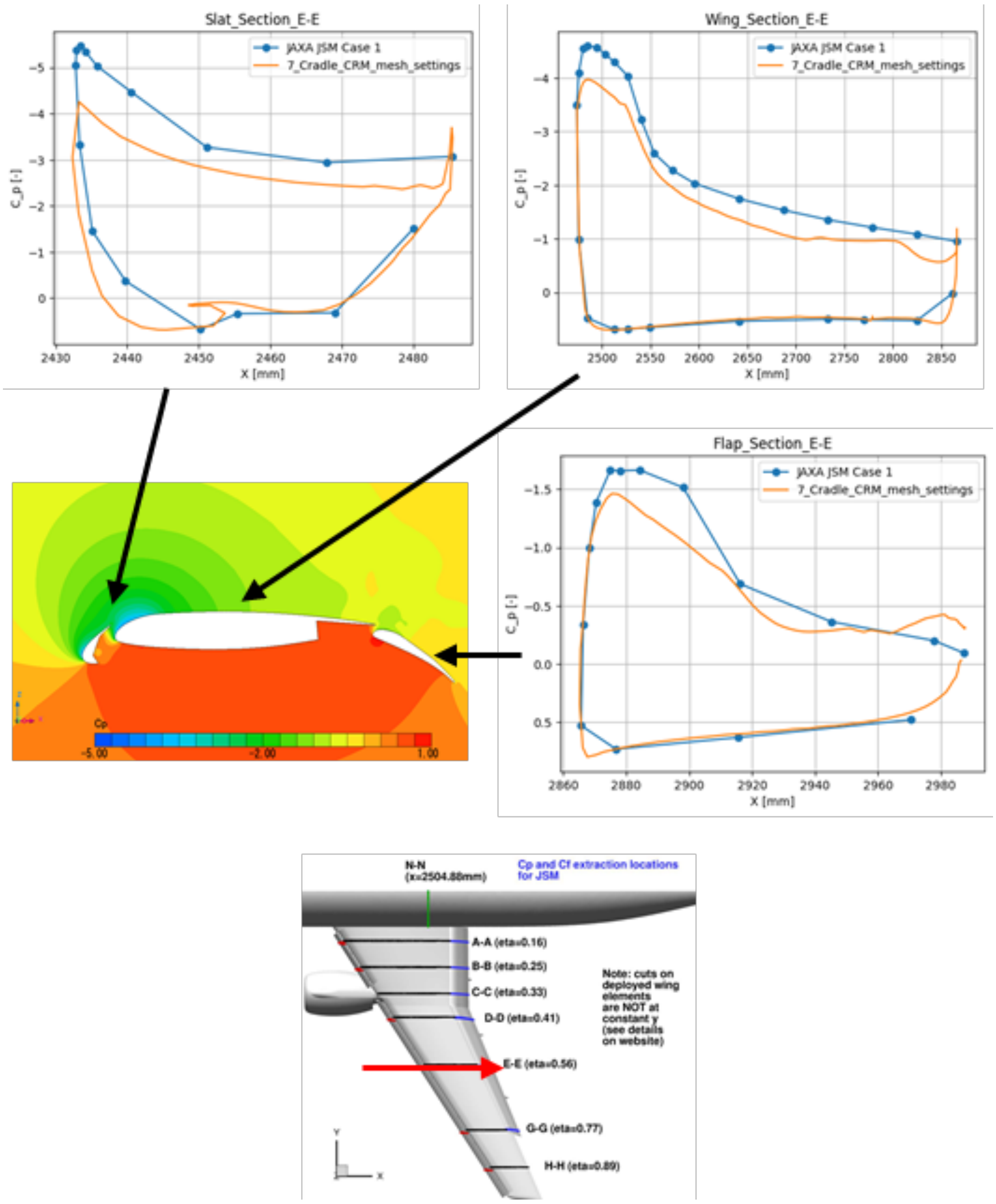

Figure 29: High lift prediction, station E-E

i. Fluid structure interaction (FSI) outer wing of glider

The final case highlights the differences of using FSI versus of a CFD-only analysis. This case represents the top of the test pyramid, as here the fully verified and validated fluid-solver is coupled with a structural solver.

The investigated case corresponds to the load on the outer wing of a glider aircraft undergoing a 4g cruise maneuver at 87.33 m/s.

Two analyses were performed and compared:

(1) CFD only analysis: Here the CFD mesh is created based on the undeformed wing configuration. The resulting pressure profile is manually mapped to the Nastran structural model and the structural analysis is performed.
(2) FSI analysis: Here again the CFD mesh is created based on the undeformed wing configuration. The resulting pressure load profile is automatically mapped to the Nastran structural model via CoSim and the structural analysis is performed. The resulting deformation are then used to automatically morph the CFD mesh to align with the deformation of the structural model. At this point the cycle starts again and is repeated until the change in structural deformation does not induce further significant change in the fluid flow.

It should be noted that the structural model can be considered a "certification grade" model. That means no simplifications on the structural model were done to accommodate the CFD simulations. The reason behind this approach is complete consistency between the structural model used to derive aerodynamic loads and the structural model used for certification later on.

The deformation of the wing based on CFD-only is shown in Figure 30, the deformation of the wing based on the FSI analysis is shown in Figure 31. It can be noted that there is a difference of about 5% with the CFD-only analysis showing smaller deformation.

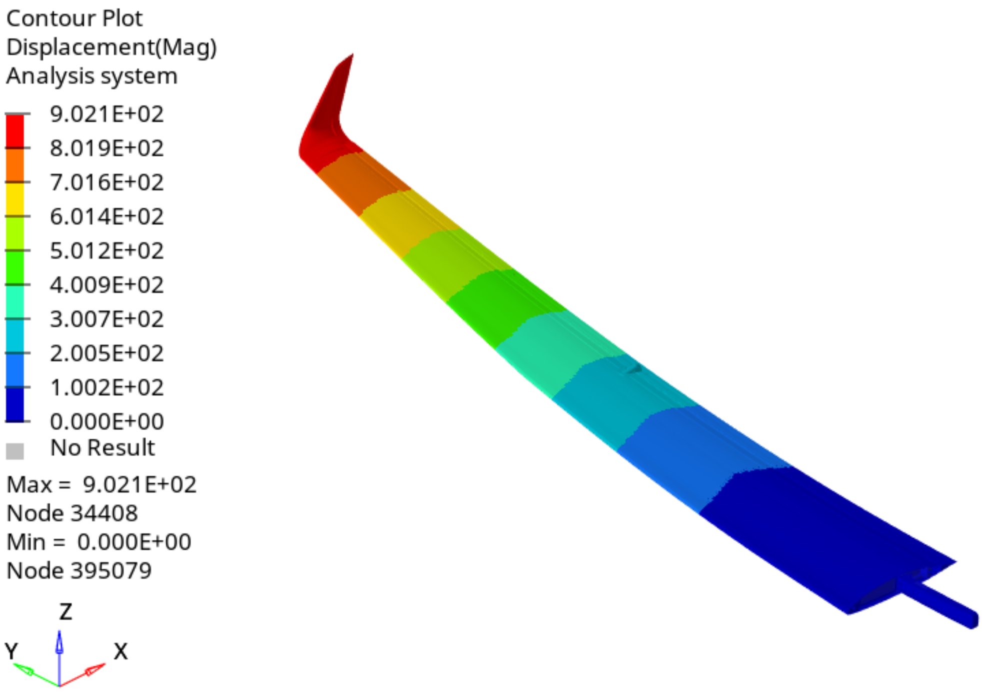

Figure 30: Deformation of wing based on CFD-only

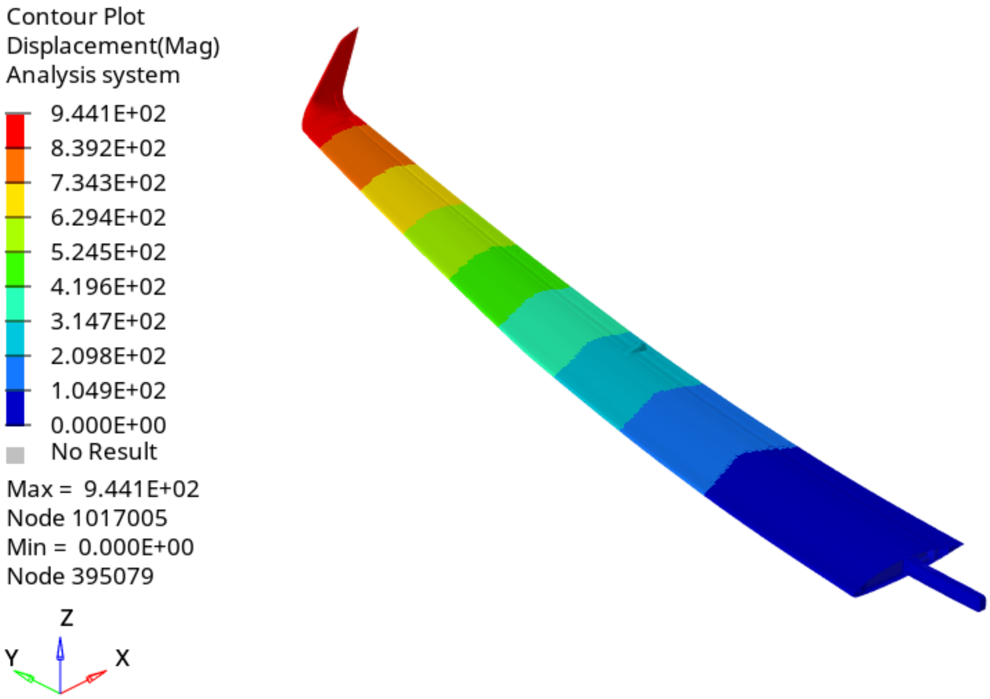

Figure 31: Deformation of wing from FSI

The cause in the change in maximum deflection becomes more apparent when looking at the pressure distribution in Figure 32 for the CFD-only analysis and in Figure 33 for the FSI analysis. It can be clearly seen that compared to the CFD-only case, the FSI case shows larger areas of negative pressure at the top but also smaller pressure at the bottom.

The reason for this lies in elementary aerodynamics for standard airfoils: An increase in lift causes a positive moment, thus increasing the lift further. This process continues until due to elastic counteracting forces a new equilibrium is achieve or aeroelastic divergence occurs.

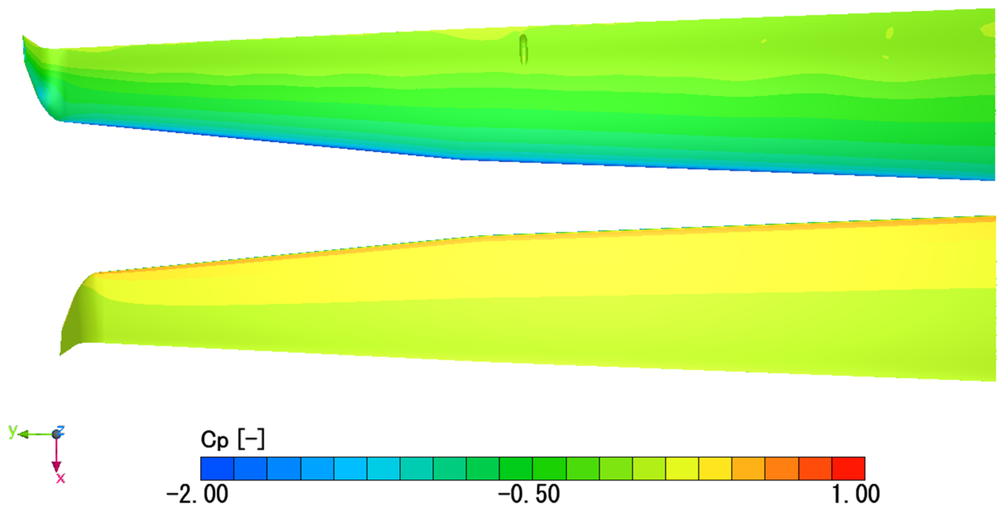

Figure 32: Pressure coefficient distribution, CFD-only

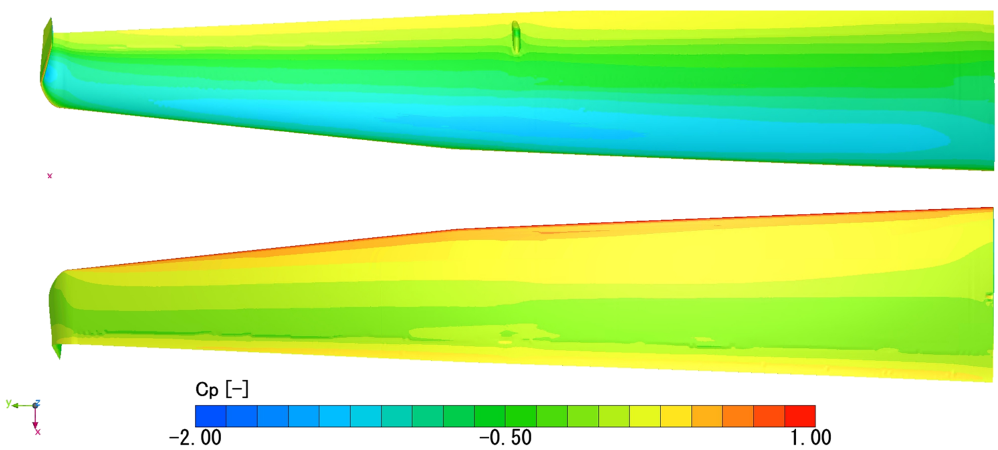

Figure 33: Pressure coefficient distribution, FSI

The morphed mesh as a result of the structural deformation is shown Figure 34.

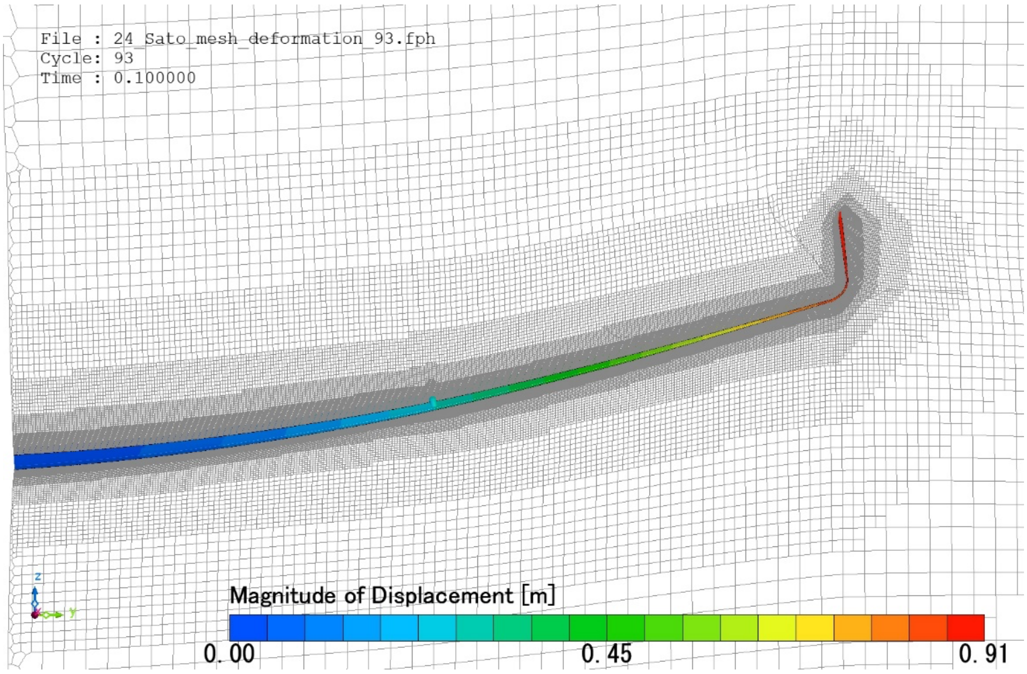

Figure 34: Morphed mesh and deformed wing in FSI simulation.

Finally, Figure 35 and Figure 36 show the minimum principle (compressive) strain distribution in the wing for the CFD-only and FSI analysis. These values can serve as a first indicator for structural load and failure. The minimum principle strain reported in the structure is 8040 µstrain for CFD-only, while it is 9337 µstrain for FSI, making a difference of 14% with CFD-only being too conservative. This highlights the need to account for large structural deflection during the fluid dynamic analysis for the presented case.

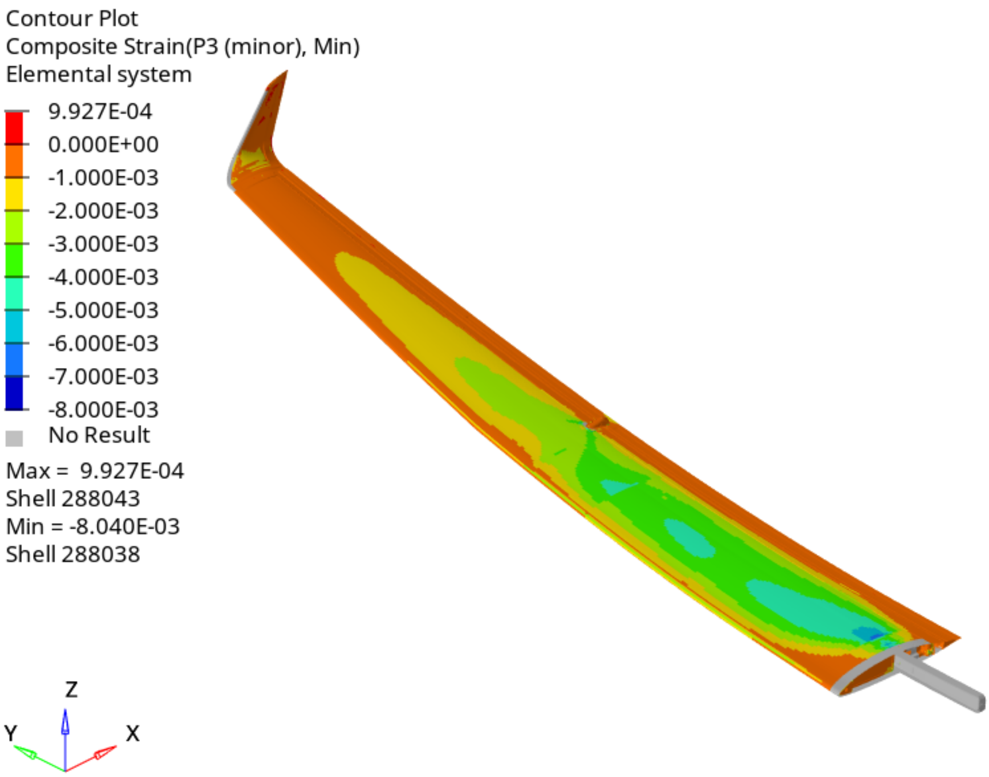

Figure 35: Minimum principle (compressive) composite strain, CFD-only

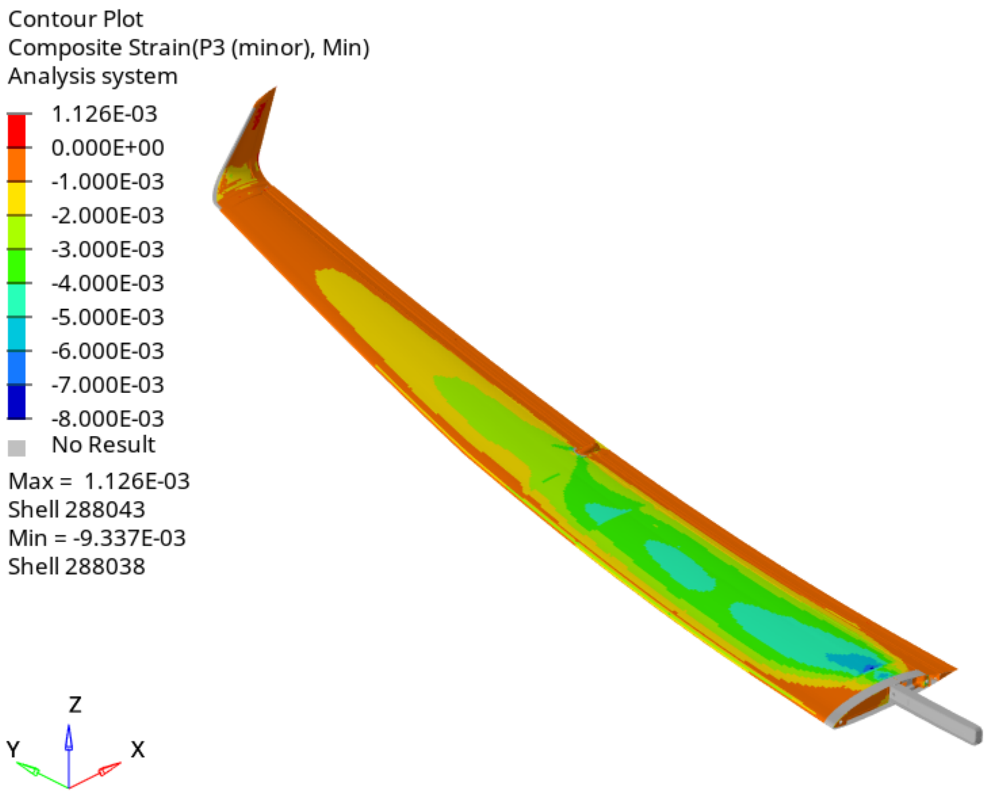

Figure 36: Minimum principle (compressive) composite strain, FSI

3. Summary

In this paper a test pyramid was presented from a fluid dynamic and aeroelastic (fluid structure interaction - FSI) viewpoint analogous to the test pyramid know from certification of aircraft structures. The aim of the presented test pyramid and the simulations along the different levels is a more Modelling and Simulation-based (M&S) approach to aircraft certification compared to what is done currently. To this end verification and validation activities were performed. Generally, good results are achieved on the different levels, thus allowing for a M&S based certification.

At the top level of the test pyramid, both structural and fluid dynamic aspects were combined in a complex FSI analysis. It was demonstrated that CFD-only results may yield too optimistic values and that for wings with large deflection that change in flow pattern due to structural deformation should be considered.

4. Acknowledgement

The presented work is supported through Luftfahrtforschungsprogramm LuFo VI-1. The project underlying this report was funded by the Federal Ministry of Commerce and Climate Change under the funding code 20W1909C. The title of the project is "PROVING - Strukturmechanische Harmonisierung und Nachweisführung für Luftfahrtkomponenten aus generativen Fertigungsverfahren." The author is responsible for the content of this publication.

The fluid and FSI simulations were performed by Hexagon Manufacturing Intelligence GmbH under subcontract from Boeing Deutschland GmbH.

5. References

[1] U.S. Department of Transportation, Federal Aviation Administration, *AC 25.307-1 Proof of structure,* 2014.

[2] T. Mauery, J. Alonso, A. Cary, V. Lee, R. Malecki, D. Mavriplis, G. Medic, J. Schaefer and J. Slotnick, "NASA/CR-20210015404 - A Guide for Aircraft Certification by Analysis," 2021.

[3] S. A. Chisholm, J. F. Castro, B. D. Chapman, K. Z. Karayev, A. J. Gunther and M. H. Kabir, "Smarter Testing Through Simulation for Efficient Design and Attainment of Regulatory Compliance," in *ICAF 2019 – Structural Integrity in the Age of Additive Manufacturing: Proceedings of the 30th Symposium of the International Committee on Aeronautical Fatigue*, Krakow, 2019.

[4] European Union Aviation Safety Agency, *Proposed CM-S-014 Issue 01 - Modelling & Simulation – CS-25 Structural Certification Specifications,* 2020.

[5] U.S. Department of Transportation, Federal Aviation Administration, *AC 20-107B - Composite Aircraft Structure,* 2009.

[6] European Union Aviation Safety Agency, *AMC 20-29 - Composite Aircraft Structure,* 2010.

[7] Software Cradle Co., Ltd., *scFLOW User's Guide Operation,* Osaka: Hexagon AB, 2024.

[8] Hexagon Manufacturing Intelligence, Inc. UK, *MSC CoSim 2024.1 - User's Guide,* Cobham: Hexagon AB, 2024.

[9] F. M. White, Viscous Fluid Flow, McGraw-Hill, Inc., 1974.

[10] NASA Glenn Research Center, "NPARC Alliance CFD Verification and Validation Website," 10 02 2021. [Online]. Available: https://www.grc.nasa.gov/www/wind/valid/archive.html. [Accessed 02 01 2025].

[11] F. M. White, Fluid Mechanics (Fourth Edition), McGraw-Hill, 1999.

[12] A.J.Wadcock, "NASA CR 177450 - Investigation of Low-Speed turbulent spearated flow around airfoils," NASA, Washington, 1987.

[13] NASA, "Langley Research Center Turbulence Modeling Resource," 10 01 2017. [Online]. Available: https://turbmodels.larc.nasa.gov/naca0012numerics_val.html. [Accessed 25 01 2025].

[14] D. H. Hodges and G. A. and Pierce, Introduction to Structural Dynamics and Aeroelasticity (2nd Edition), Cambridge: Cambridge University Press, 2011.

[15] S. Turek and J. Hron, "Proposal for Numerical Benchmarking of Fluid-Structure Interaction between an Elastic Object and Laminar Incompressible Flow," in *Bungartz, HJ., Schäfer, M. (eds) Fluid-Structure Interaction. Lecture Notes in Computational Science and Engineering, vol 53.*, Berlin, 2006.

[16] V. Mineck, “Wind-tunnel investigation of aerodynamic efficiency of three planar elliptical uings hith curvature of quarter-choro line,” NASA, 1993.

[17] AIAA, “3rd AIAA CFD High Lift Prediction Workshop (HiLiftPW-3),” 22 02 2023. [Online]. Available: https://hiliftpw.larc.nasa.gov/. [Accessed 25 01 2025].

[18] F.R.Mentner, “Two-equation eddy-viscosity turbulence models for engineering applications,” *AIAA Journal,* vol. 32, no. 8, 1994.

[19] Y. A. Çengel and J. M. Cimbala, Fluid Mechanics - Fundamentals and, McGraw-Hill Education, 2018.